^{31}P and ^{2}H Relaxation Studies of Helix VII and the Cytoplasmic Helix of the Human Cannabinoid Receptors Utilizing Solid-State NMR Techniques†

Elvis K. Tiburu,‡ Ethan S. Karp,§ Gabriel Birrane,‡ Jochem O. Struppe,|| Shidong Chu,§ Gary A. Lorigan,§ Shalom Avraham,‡ and Hava Karsenty Avraham*,‡

Division of Experimental Medicine, Beth Israel Deaconess Medical Center, Harvard Medical School, Boston, Massachusetts 02115, NMR Division, Bruker Biospin Corporation, Billerica, Massachusetts 01821, and Department of Chemistry and Biochemistry, Miami University, Oxford, Ohio 45056

Received December 19, 2005; Revised Manuscript Received April 21, 2006

ABSTRACT: Cannabinoid receptors are G-protein-coupled receptors comprised of seven transmembrane helices. We hypothesized that the extended helix of the receptor interacts differently with POPC bilayers due to the differing distribution of charged amino acid residues. To test this, hCB$_1$(T377−E416) and hCB$_2$(K278−H316) peptides were studied with ^{31}P and ^{2}H solid-state NMR spectroscopy by incorporating them into 1-palmitoyl-2-oleoyl-*sn*-glycerophosphocholine bilayers. Lipid affinities of the 40- and 39-residue peptides were analyzed on the basis of ^{31}P and ^{2}H spectral line shapes, order parameters, and T_1 relaxation measurements of the POPC bilayers. Lipid headgroup perturbations were noticed in the ^{31}P NMR spectra in the lipid/peptide mixtures when compared with the pure lipids. ^{2}H order parameters were calculated from the quadrupolar splitting of the de-Paked ^{2}H NMR spectra. At the top of the acyl chain, pure lipids had an average $S_{CD} \approx 0.20$, whereas $S_{CD} \approx 0.16$ and $S_{CD} \approx 0.18$ were found in the presence of hCB$_1$(T377−E416) and hCB$_2$(K278−H316), respectively. S_{CD} values decreased in the central part of the acyl chains when compared to the pure POPC lipids, indicating a change in the dynamic properties of the lipid membrane in the presence of the cannabinoid peptides. R_{1Z} vs S^2_{CD} plots exhibited a linear dependency with and without the peptides, with an increase in slope upon addition of the peptides to the POPC, indicating that the dynamics of the lipid bilayer is dominated by fast axially symmetric motion. This study provides insights into the interaction of cannabinoid peptides with the membrane bilayer by investigating the headgroup and acyl chain dynamics.

In solid-state NMR[1] spectroscopy, broad signals are observed because of the anisotropy of the chemical shielding and the dipolar and quadrupolar interactions (*1*−*6*). This technique has been widely used to analyze the structure and dynamic properties of peptides as well as macromolecules, including those that associate with membranes or biomineral surfaces (*7*−*10*). Solid-state NMR spectroscopy is also becoming a leading tool for the study of membrane protein interactions with lipids. The anisotropy inherent in such broad line solid-state NMR spectra has been used to describe molecular interactions between lipids and proteins at the membrane interface (*11*). The most common nuclei used as probes for studying chemical shift anisotropy (CSA) interactions in the lipid headgroup of POPC are the endogenous ^{31}P nuclei present in the headgroups of the lipids. In contrast, the quadrupolar interactions of the hydrophobic core of the bilayers can be probed using the chemically nonexchangeable ^{2}H nucleus, which can be added synthetically to a specific position on the lipid molecule.

The central nervous system contains phospholipids and signaling receptors, such as the cannabinoid receptor 1 (CB$_1$), that are involved in signal transduction (*12*−*14*). There are at least two types of cannabinoid receptors (CB$_1$ and CB$_2$) that are G-protein-coupled receptors (GPCRs) stimulated by cannabinoid agonists such as aminoalkylindole, eicosanoid ethanolamine, and esters (*15*). The CB$_1$ receptor is predominantly present in the central nervous system and is expressed in many regions of the brain including the hippocampus, cerebral cortex, basal ganglia, and cerebellum (*16*, *17*). The CB$_2$ receptor is found in certain peripheral tissues such as the spleen and white blood cells. There is also evidence of the presence of CB$_1$ in these tissues (spleen, T cells, and B cells) (*18*, *19*). The concept of organized trafficking of lipids

† This work was supported by an NRSA Training Grant, HL07917-06 (to E.K.T.), from the National Institutes of Health and NCI Grant CA96805 (to H.K.A.). A National Institutes of Health Grant (GM60259-01) and National Science Foundation CAREER Award (CHE-0133433) also supported this work (to G.A.L.). The 500 MHz wide-bore NMR spectrometer was obtained from a National Science Foundation grant (10116333). E.S.K. acknowledges the Arnold O. Beckman Foundation for financial support.

* Correspondence should be addressed to this author. Phone: (617) 667-0073. Fax: (617) 975-6373. E-mail: havraham@bidmc.harvard.edu.

‡ Harvard Medical School.

§ Miami University.

|| Bruker Biospin Corp.

[1] Abbreviations: FMOC, 9-fluorenylmethoxycarbonyl; GPCR, G-protein-coupled receptor; HEPES, 4-(2-hydroxyethyl)-1-piperazineethanesulfonic acid; hCB, human cannabinoid receptor; MALDI-TOF, matrix-assisted laser desorption ionization time of flight; NMR, nuclear magnetic resonance; POPC, 1-palmitoyl-2-oleoyl-*sn*-glycerophosphocholine; R_{1Z}, relaxation rate; TFE, 2,2,2-trifluoroethanol; T_{1Z}, relaxation time.

10.1021/bi0525831 CCC: $33.50
Published on Web 05/19/2006

in the presence of cannabinoid receptors is very controversial. There are models that tend to speculate on the involvement of lipid rafts and their related caveolae family in ligand trafficking (*20*, *21*).

The cannabinoid receptors are among the most important GPCRs for drug discovery. However, our understanding of their mode of action has been hindered by the lack of a three-dimensional structure. The cytoplasmic helix (helix VIII) of the cannabinoid receptors has been implicated to bind to G-proteins when activated by ligand binding. In its restive state, helix VIII is presumed to bind to phospholipid bilayers with the long axis of the helix being perpendicular to the bilayer normal which is probably tethered to the membrane surface due to palmitoylation at cysteine sites. Other GPCR receptors (though not in the cannabinoid superfamily), such as the histamine receptor, dopamine receptor, and mastoparan X, have been found to behave in a similar manner (*22*).

The only existing known structures of CB_1 and CB_2 are from computer molecular modeling studies based upon the crystal structure of a related GPCR protein (bovine rhodopsin) (*23*, *24*). The crystal structure of family I rhodopsin-like GPCRs has been determined, and important structural features were revealed concerning all GPCRs (*25*). In the rhodopsin structure, helix VIII is characterized and can be compared to helix VIII in the cannabinoid receptors. The orientation of helix VII within the bilayer of rhodopsin is dictated by a conformational change in helix VIII (*26*). This conformational change is governed by either the surrounding environment or the interaction of the polar residues with the lipid headgroups. Although strides have been made to model CB_1 and CB_2, structurally, the CB_1 and CB_2 receptors exhibit several intriguing anomalies which place these receptors in a subset of type 1 GPCRs. Some of these anomalies include relatively long N- and C-termini, which may be involved in receptor stability. To understand the lipid/peptide interactions and obtain a better three-dimensional perspective of helix VII and helix VIII in CB_1 and CB_2, the extended (helix VII and the cytoplasmic α-helical domain) synthetically created CB_1 and CB_2 peptides were made and incorporated into model phospholipid membranes. The motions of the headgroup as well as the hydrocarbon chain of the phospholipids were monitored using ^{31}P and ^{2}H NMR spectroscopic techniques. In addition, these studies describe the differences and similarities between CB_1 and CB_2 lipid interactions. An important consideration that is explored here in this study is whether differences in helix VIII in both receptors could serve as potential sites for a conformational bend or twist of the peptides within the membrane, resulting in increased membrane permeability, and how this might relate to the mechanism of cannabinoid action. It is important to note that the current experiments are not designed to determine the orientation of the peptides in the membrane but rather to compare their influence on the lipid headgroup and the corresponding lipid acyl chain dynamics.

EXPERIMENTAL PROCEDURES

Materials. 1-Palmitoyl-2-oleoyl-*sn*-glycerophosphocholine lipids (POPC and POPC-d_{31}), already dissolved in chloroform, were purchased from Avanti Polar Lipids (Alabaster, AL) and stored at −20 °C prior to use. 2,2,2-Trifluoroethanol (TFE), 4-(2-hydroxyethyl)-1-piperazineethanesulfonic acid (HEPES), and EDTA were obtained from Sigma-Aldrich (Milwaukee, WI). Deuterium-depleted water was purchased from Sigma-Aldrich. All other chemicals were purchased from Sigma-Aldrich.

Peptide Synthesis and Purification. Peptides corresponding to helix I and helix VII of CB_1, hCB_1(A118−L147) and hCB_1(T377−E416), respectively, as well as helix VII of CB_2, hCB_2(K278−H316), were synthesized using an Applied Biosystems peptide synthesizer (ABI 433A) equipped for FMOC chemistry at the Molecular Biology Core Facility, Dana-Farber Cancer Institute. All amino acids were single coupled, with a total of 9.5 min for the coupling and monitoring module. The crude peptide was purified on a two Dynamax Model, SD-200 high-performance liquid chromatography system, controlled by an Applied Biosystems 1000S diode array detector. The software used was Dynamax Method Manager version 1.4.6. The purified peptide was analyzed by MALDI-TOF using a calibration matrix of α-cyano-4-hydroxycinnamic acid at the Molecular Biology Core Facility, Dana-Farber Cancer Institute.

NMR Sample Preparation. Bilayers of POPC were prepared with various mole percentages of peptide to lipid ratios according to a slightly modified protocol from the literature (*27*). Stock standard solutions (76 mg) of 1-palmitoyl-2-oleoyl-*sn*-glycerophosphocholine lipids in chloroform were mixed with the suitable amount of peptide dissolved in TFE to give the desired molar composition. The solvents were removed under a steady stream of N_2 gas in a 12 × 75 mm test tube at ambient temperature. For a complete dry sample, the test tube containing the sample was placed in a vacuum desiccator overnight. The dry lipid or lipid/peptide mixture was then fully rehydrated by vortexing in 190 μL of HEPES buffer (5 mM EDTA, 20 mM NaCl, and 30 mM HEPES, pH 7.0) and heating in a water bath at 50 °C with occasional sample agitation. The sample was occasionally frozen and then thawed by placing it in liquid nitrogen and at room temperature alternatively to reduce sample frothing while mixing. All samples were prepared with deuterium-depleted water (Sigma-Aldrich). The fully homogeneous lipid/peptide suspension was transferred to an NMR sample rotor. To obtain a well-packed sample, the rotor was spun in an Eppendorf tube. For the ^{2}H NMR experiments, 5 mg of POPC-d_{31} was used as an isotopic label with the excess nonlabeled POPC.

NMR Spectroscopy. NMR spectra were obtained on a Bruker-Biospin Avance 500 MHz solid-state NMR spectrometer operating at 202.5 MHz for ^{31}P and 76.8 MHz for ^{2}H. A double resonance 5 mm round coil probe was used for spectra collection (Bruker, Billerica, MA). The spectrometer setup conditions consisted of either a direct polarization (short single $\pi/2$ pulse) of 4 μs and 5 s recycle delay with ^{1}H decoupling or a phase-cycled Hahn-echo pulse sequence for ^{31}P NMR. The samples were run with the Hahn-echo pulse sequence under the same experimental conditions for comparison with the single pulse data. A total of 1024 transients were taken, and the free induction decay was processed using 100 Hz line broadening. The spectral width was set to 150 ppm. The ^{2}H quadrupolar echo pulse sequence was used with quadrature detection accompanied by complete phase cycling of the pulse pairs (*28*). The 90° pulse was 3 μs, the interpulse delay was 20 μs, and the recycle delay was 0.3 s. The spectral width was set to 100 kHz, and a

(I) hCB_1(A118-L147) -A-I-A-V-L-S-L-T-L-G-T-F-T-V-L-G-N-L-L-V-L-C-V-I-L-H-S-R-S-L

(II) hCB_1(T377-E416)- T-V-F-A-F-C-S-M-L-C-L-L-N-S-T-V-N-P-I-I-Y-A-L-R-S-K-D-L-R-H-A-F-R-S-M-F-P-S-C-E

(III) hCB_2(K278-H316)- K-K-A-F-A-F-C-S-M-L-C-I-I-N-S-M-V-N-P-V-I-Y-A-L-R-S-G-E-I-R-S-S-A-H-H-C-L-A-H

FIGURE 1: Amino acid sequences of synthetic hCB_1(A118−L147), hCB_1(T377−E416), and hCB_2(K278−H316). (I) hCB_1(A118−L147) (helix I): the amino acid sequence corresponding to helix I of CB_1. (II) hCB_1(T377−E416) and (III) hCB_2(K278−H316): the amino acid sequences representing helix VII and helix VIII of CB_1 and CB_2, respectively. The numbers correspond to the position of the amino acids in the wild-type receptors. The putative transmembrane domains are underlined. The amino acids are read from the N-terminus (starting from the left) to the C-terminus (ending on the right).

total of 12000 transients were averaged for each spectrum and processed with 200 Hz line broadening. Spin−lattice relaxation times (T_{1Z}) were obtained by the inversion−recovery technique with the pulse sequence 180°−T−90°−τ−90°−τ−acquire, where T is a set of variable delays used to determine T_{1Z}.

NMR Spectra Analysis. The ^{31}P spectra were simulated with the DMFIT software program, which is capable of fitting 1D and 2D spectra (*29*). The ^{2}H NMR spectra consist of overlapping powder patterns which make it difficult to identify the resonance arising from a one-labeled position. The ^{2}H powder pattern spectra were therefore deconvoluted using an algorithm from the literature (*30*, *31*). The spectra were deconvoluted such that the bilayer normal was perpendicular to the direction of the static magnetic field tensor. The quadrupolar splitting from the deconvoluted spectra was directly measured and the order parameter calculated using the following established expression from the literature (*32*, *33*):

$$\Delta\nu_Q^{\,i} = {}^3/_4(e^2qQ/h)S^i_{CD} \quad (1)$$

In this expression, $\Delta\nu_Q^{\,i}$ is the quadrupolar splitting for a deuteron attached to the ith carbon along the acyl chain and e^2qQ/h is the quadrupolar coupling constant of 168 kHz for a deuteron in the C−^{2}H bond. S^i_{CD} measures the degree of motional restriction of the deuteron on the ith C−^{2}H bond along the acyl chain segment.

The variable T delays used for the T_{1Z} measurements were fitted using the exponential function:

$$I(t) = I(0)[1 - A\exp(-T/T_{1Z})] \quad (2)$$

where $I(t)$ is the change in peak intensity as a function of the variable T delay (varied from 1 ms to 7 s) used to calculate T_{1Z}. A is a fitting parameter and is close to 2, and $I(0)$ is about 1 (*34*). The ^{2}H spin−lattice relaxation rate, R_{1Z}, is related to T_{1Z} by $R_{1Z} = 1/T_{1Z}$, and the standard deviation for each R_{1Z} value was about ±0.004 ms.

RESULTS

The amino acid sequences corresponding to the human cannabinoid receptors, hCB_1(A118−L147), hCB_1(T377−E416), and hCB_2(K278−H316), are shown in Figure 1. The sequences represent helix I of CB_1, as well as helix VII and the juxtamembrane segment of CB_1 and CB_2. As shown in Figure 1, the transmembrane segment of the two peptides (II and III) has >80% sequence identity with only small differences (e.g., the hCB_2 peptide has contiguous lysines at the N-terminus), and the corresponding amino acids at the N-terminus of hCB_1 are threonine and valine. The major differences between the peptides occur in the C-terminal juxtamembrane region (helix VIII). The amphipathic characteristics of the juxtamembrane segment have interesting structural and functional properties and are commonly observed in other GPCRs.

The interactions between the cannabinoid receptors and lipids at the lipid−water interfaces as well as within the hydrophobic core were studied with solid-state NMR spectroscopy by utilizing endogenous ^{31}P at the lipid headgroup and an isotopically enriched ^{2}H label along one of the acyl chains of the 1-palmitoyl-2-oleoyl-*sn*-glycerophosphocholine lipid. The choline headgroup of POPC can report some changes in electrical charge at the bilayer surface, causing changes in the orientation of the phospholipid headgroup. As shown in Figure 2A,B, the ^{31}P NMR spectra were recorded from 30 to 60 °C for POPC with hCB_1(T377−E416) or POPC with hCB_2(K278−H316). The solid line spectra represent the ^{31}P NMR spectra of the POPC bilayers with 1 mol % hCB_1(T377−E416), whereas the dashed line spectra in Figure 2A represent the ^{31}P NMR spectra of POPC without the peptide. The motionally averaged powder pattern spectra of Figure 2A (dashed line) are characteristic of the phospholipid bilayers in the liquid-crystalline L_α phase as well as of the POPC bilayers well above their chain melting transition temperature of −3 °C (*35*). Upon addition of 1 mol % peptide, the local motion at the headgroup is increased, but there is very little change in the axially symmetric line shapes (where $\sigma_{33} > \sigma_{22} \approx \sigma_{11}$) (solid line). The characteristic spectral line shapes in the presence of the peptide indicate that the phospholipid bilayers remain in the L_α phase even after the addition of 1 mol % hCB_1(T377−E416) at all temperatures. However, the increase in local motion at the headgroup is manifested in a slightly reduced chemical shift anisotropy (CSA) width of the spectra at all temperatures. The CSA for the POPC bilayers was approximately 45 ± 0.5 ppm and that of the POPC with 1 mol % hCB_1(T377−E416) was about 41 ± 0.5 ppm at 30 °C, as shown in Figure 2A. When the experiments were repeated with hCB_2(K278−H316), the line shapes also indicated an intact phospholipid bilayer at a 1 mol % concentration of the peptide as shown in Figure 2B. The CSA for POPC was approximately 45 ± 0.5 ppm and that of the POPC with 1 mol % hCB_2(K278−H316) was about 43 ± 0.5 ppm at 30 °C. There is also a reduction in the CSA width at all temperatures in the presence of hCB_2(K278−H316). It is difficult to decipher the magnitude of POPC lipid perturbation induced by the presence of hCB_1(T377−E416) and hCB_2(K278−H316) from the ^{31}P NMR spectra. The most important information is derived from the approximate axially symmetric line shapes (where $\sigma_{33} > \sigma_{22} \approx \sigma_{11}$) at all temperatures for both POPC with hCB_1(T377−E416) and POPC with hCB_2(K278−H316) in the L_α phase. For comparison, the spectra corresponding to POPC in the absence of the peptides and POPC with 1 mol % peptides at 30 °C were superimposed as shown in Figure 2C. The axially symmetric line shapes are clearly shown, and it can be seen that perturbation of the POPC bilayer is slightly more significant in the presence of hCB_1(T377−E416) than hCB_2-

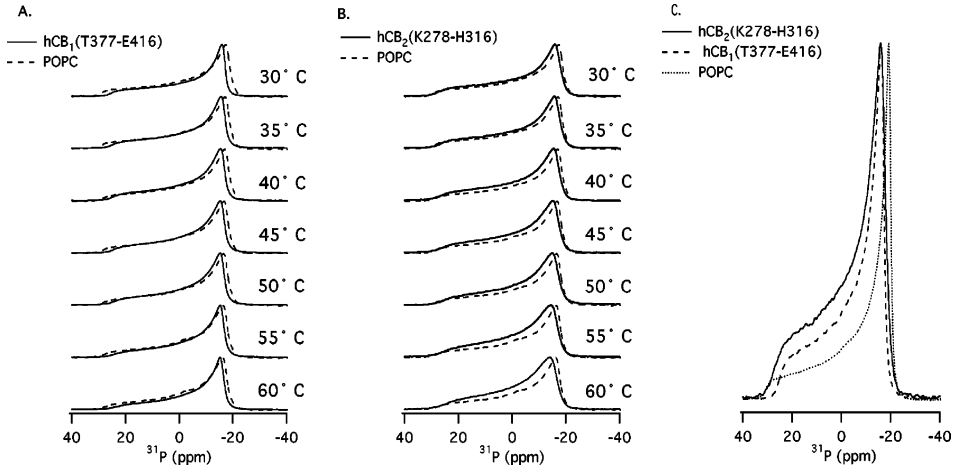

FIGURE 2: ^{31}P NMR spectra of 1 mol % peptides interact with the POPC headgroup investigated as a function of temperature. (A) The spectra shown with solid lines represent POPC with 1 mol % hCB_1(T377−E416), and the dashed lines represent POPC lipid bilayers prepared in the absence of peptide. (B) The spectra shown with the solid lines represent POPC with 1 mol % hCB_2(K278−H316), and the dashed lines represent POPC lipid bilayers prepared in the absence of peptide. The spectra were collected starting at 30 °C, in 5 °C increments. (C) ^{31}P NMR spectra of endogenous phosphorus at the headgroup of POPC lipid bilayers (dotted line), POPC with 1 mol % hCB_1(T377−E416) (dashed line), and POPC with 1 mol % hCB_2(K278−H316) (solid line).

(K278−H316) as indicated by the small ^{31}P CSA span of the lipids containing the former peptide. At 1−2 mol % peptide concentrations, there was little change in the ^{31}P spectral shape, except for the differences in CSA width between the two peptides.

Next, the ^{31}P NMR spectra consisting of POPC bilayers containing up to 4 and 6 mol % peptides were investigated. At 4 mol %, the ^{31}P NMR spectra revealed several different spectroscopic components including an isotropic peak centered around 0 ppm as shown in Figure 3A [4 mol % hCB_1(T377−E416)] and Figure 3C [4 mol % hCB_2(K278−H316)]. Similar results were obtained for POPC with 6 mol % peptide (data not shown). The isotropic component is more pronounced in POPC with 4 mol % hCB_1(T377−E416) (Figure 3A), when compared to POPC with 4 mol % hCB_2(K278−H316) (Figure 3C). The appearance of an isotropic peak close to 0 ppm was observed at all temperatures and probably indicates the complete averaging of the anisotropies induced by the micellar components. The isotropic peak may also indicate the existence of other lipid phases. The spectral line shapes indicate the presence of additional axially symmetric components (Figure 3A,C). The spectra at 30 °C were actually simulated and the small vesicles identified for POPC with hCB_1(T377−E416) (Figure 3B) and POPC with hCB_2(K278−H316) (Figure 3D). The diameters of the vesicles were calculated from the CSA widths for different multilamellar vesicle (MLV) species using the approach of Burnell et al. (*36*). At 1 mol % peptide with respect to POPC, larger MLVs with an approximate diameter of 25000 ± 11 Å were formed (CSA ∼ 45 ppm). At 4 mol % peptide with respect to POPC, vesicles with diameters of 20000 ± 7 (CSA ∼ 35 ppm), 5000 ± 4 (CSA ∼ 28 ppm), and 2000 ± 5 (CSA ∼ 18 ppm) and one isotropic component with a diameter of 500 ± 3 Å (CSA ∼ 4 ppm) appeared in both spectra (Figure 3B,D). The contributions from the 20000, 5000, 2000, and 500 Å vesicles were 76 ± 1%, 12 ± 1%, 9 ± 1%, and 3 ± 0.5%, respectively, for POPC with hCB_1(T377−E416) and 81 ± 2%, 12 ± 1%, 6 ± 1%, and 1 ± 0.5%, respectively, for POPC with hCB_2(K278−H316). The 6 mol % peptide gave similar results as the 4 mol % peptide (data not shown).

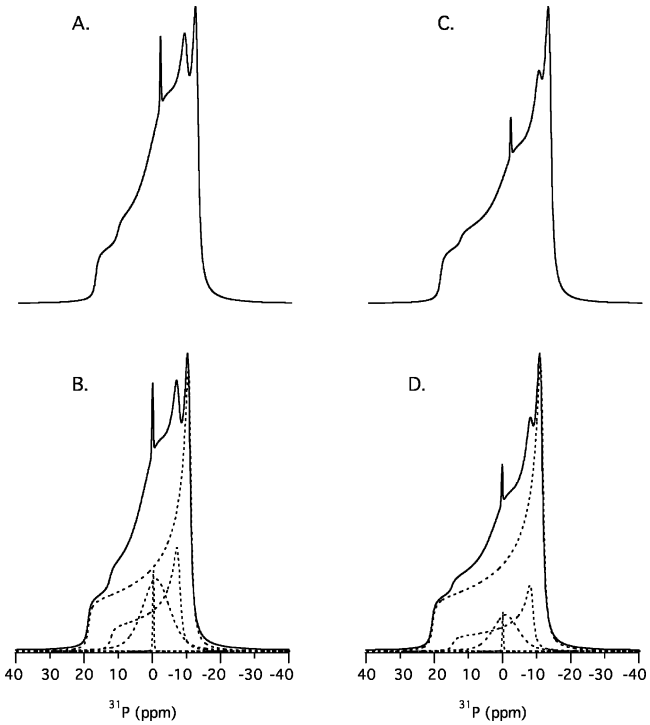

FIGURE 3: ^{31}P NMR spectra of POPC phospholipid bilayers in the presence of 4 mol % cannabinoid peptides. (A) Experimental ^{31}P NMR spectra of POPC with 4 mol % hCB_1(T377−E416). (B) The simulated POPC data with 4 mol % hCB_1(T377−E416). The dotted line spectra represent bilayer species having different vesicle sizes possessing different CSA widths. The solid line spectra are the summation of all of the species and represent the best fit for the experimental data. (C) Experimental spectra of POPC with 4 mol % hCB_2(K278−H316). (D) The simulated POPC data with 4 mol % hCB_2(K278−H316). Same explanation as in (B) except in the presence of hCB_2(K278−H316).

The difference in the percentage of the isotropic component (of 2%) may indicate that the CB_2 peptide induces less disordering on the lipid headgroup when compared to its isoform.

^{2}H NMR data of acyl chain perdeuterated POPC were obtained by incorporating the peptides into a POPC bilayer

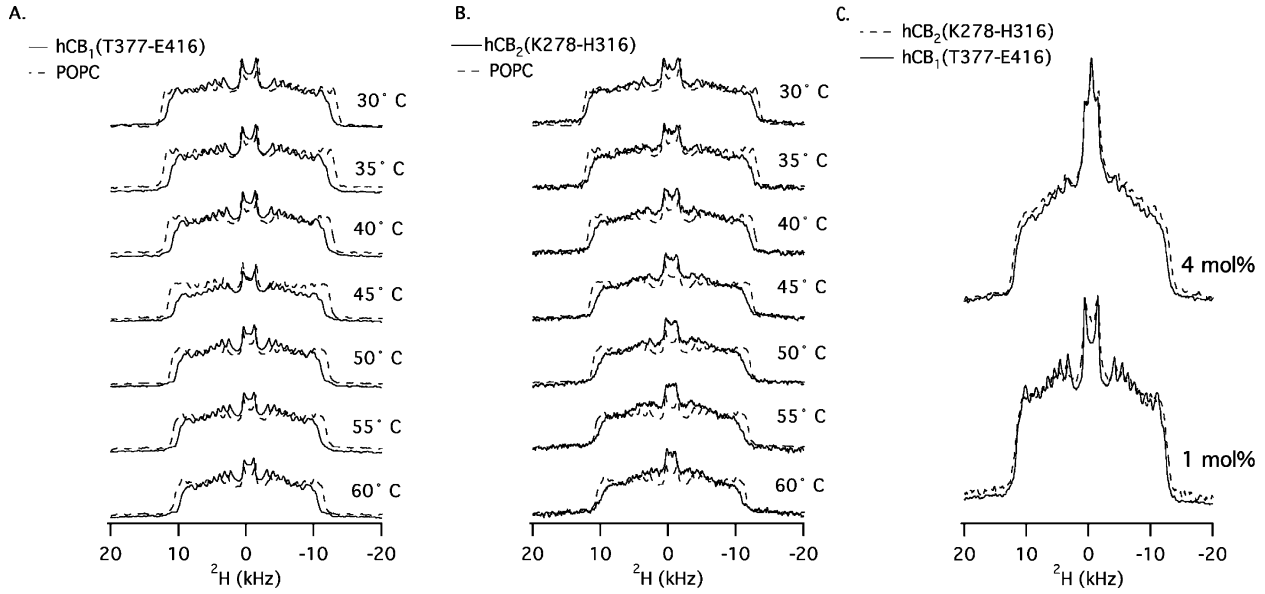

FIGURE 4: ^{2}H NMR spectra of the interaction of the POPC acyl chain with cannabinoid peptides investigated as a function of temperature. (A) The spectra shown with the solid lines represent temperature-dependent ^{2}H NMR spectra of isotopically labeled POPC with 1 mol % hCB_1(T377−E416), and spectra with the dotted lines represent POPC bilayers prepared in the absence of peptide. (B) The spectra shown with the solid lines represent ^{2}H NMR spectra of isotopically labeled POPC with 1 mol % hCB_2(K278−H316), and the dotted line spectra represent POPC lipid bilayers prepared in the absence of peptide. The spectra were collected starting at 30 °C, in 5 °C increments. (C) ^{2}H solid-state NMR spectra of isotopically labeled POPC-d_{31} with 1 mol % hCB_1(T377−E416) (solid line) and POPC with 1 mol % hCB_2-(K278−H316) (dotted line). The spectra were recorded at 30 °C for comparison.

doped with POPC-d_{31}, as described in the Experimental Procedures section. Incorporation of hCB_1(T377−E416) into the POPC bilayers induced a decrease in the acyl chain quadrupolar splitting when compared to the pure POPC bilayers (Figure 4A). It is important to note that the ^{2}H NMR spectra had characteristic axially symmetric powder pattern line shapes which were maintained at all temperatures. These line shapes were observed as a result of the motions of the phospholipids about the bilayer normal giving rise to overlapping doublet resonances that culminated from the different CD_2 segments of the acyl chain. The doublet close to 0 kHz corresponds to CD_3 at the terminal acyl chain having the most motion. Qualitatively similar variations were observed when the hCB_2(K278−H316) peptide was incorporated into the POPC bilayers (Figure 4B). As clearly observed, within the limits of experimental error (±1 kHz), there was an overall decrease in quadrupolar splitting upon incorporation of the peptide. A comparison was made between the influences of the two peptides on the acyl chains of the POPC bilayer at 30 °C, as shown in Figure 4C. POPC with hCB_2(K278−H316), as represented by the dotted lines, has slightly larger quadrupolar splitting compared to the POPC with hCB_1(T377−E416) (represented by the solid lines) at 1 and 4 mol % peptide concentrations. However, an isotropic component can be seen in the POPC spectra with a concentration of 4 mol % peptide, probably due to the bilayer fragmentation observed with the simulated ^{31}P NMR spectra (Figure 3B,D). The additional lysine residues in hCB_2(K278−H316) appear to further broaden the spectra when compared to hCB_1(T377−E416) at both the 1 and 4 mol % peptide concentrations.

The smooth segmental C−D bond order parameters (S_{CD}), which provide a means of determining the motional restriction, were calculated at 30 °C from the de-Paked spectra of the pure POPC lipids and differed from the POPC/peptide mixtures (Figure 5). Since the multibody interactions present within the lipid/peptide system can complicate determination of the segmental order parameters, the values of the order parameters were displayed with the assumption that the static quadrupolar interaction tensor for the C−D bond was axially symmetric. As shown in Figure 5, there was a characteristic profile of decreasing order toward the methyl group of the acyl chain. The order parameter S_{CD} of pure POPC of up to

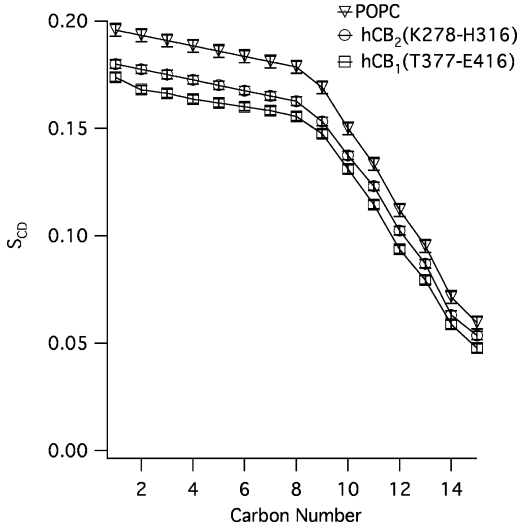

FIGURE 5: S_{CD} ordering of the POPC acyl chain in the presence of the cannabinoid peptides. Orientational order parameter (S_{CD}) profile of POPC-d_{31} with 1 mol % hCB_1(T377−E416) or with 1 mol % hCB_2(K278−H316) and POPC-d_{31} lipid bilayers prepared in the absence of peptide. The S_{CD} was calculated from the quadrupolar splittings obtained from the de-Paked spectra at 30 °C. The S_{CD} was calculated starting from the methyl deuteron at the end of the acyl chain toward the methylene close to the POPC headgroup. The uncertainty in the measurements is about ±0.002 for triplicate data points.

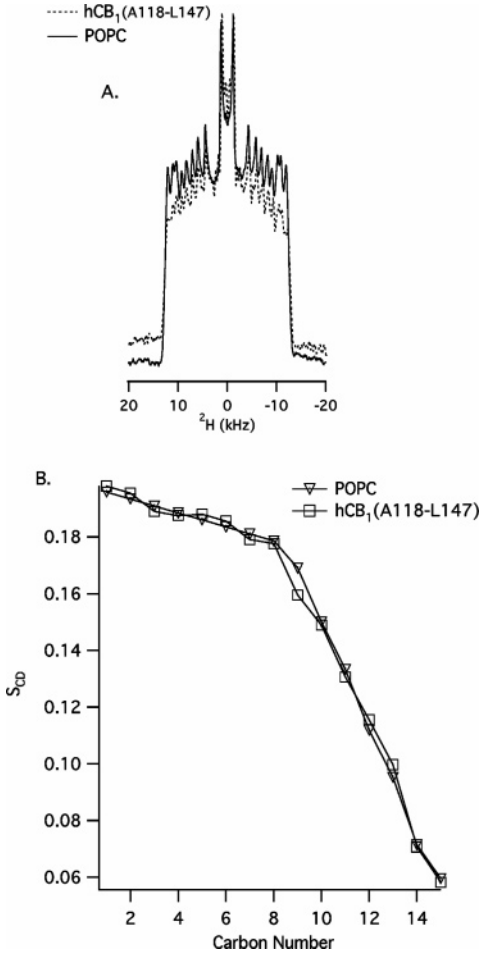

FIGURE 6: ^{2}H solid-state NMR spectra and S_{CD} of the POPC acyl chain in the presence of hCB$_1$(A118−L147). (A) Temperature-dependent ^{2}H NMR spectra of isotopically labeled POPC with 1 mol % hCB$_1$(A118−L147). The spectrum shown with the solid line is POPC with hCB$_1$(A118−L147). The spectrum shown with the dotted line represents POPC lipid bilayers prepared in the absence of peptide. (B) Orientational order parameter (S_{CD}) profile of POPC-d_{31} with 1 mol % hCB$_1$(A118−L147) and POPC-d_{31} lipid bilayers prepared in the absence of peptide.

$\sim$0.20 $\pm$ 0.002 is in good agreement with previous studies by Huber et al. (*37*). The S_{CD} profile of POPC with the two peptides was different than the pure lipid, as the POPC with hCB$_1$(T377−E416) ($S_{CD} \sim 0.16 \pm 0.002$) showed a greater disordering effect of the lipid acyl chain when compared to the hCB$_2$(K278−H316) ($S_{CD} \sim 0.18 \pm 0.002$) peptide.

To test whether the POPC acyl chain dynamics are unique to helix VII of the cannabinoid receptors, we incorporated a synthetic peptide corresponding to helix I of CB$_1$ [hCB$_1$-(A118−L147)] into POPC at a 1 mol % peptide to lipid ratio (Figure 6). The results shown in Figure 6A indicate no significant perturbation of the acyl chain dynamics upon incorporation of the peptide into the POPC. Unlike in Figure 4A,B, there was no overall decrease in quadrupolar splitting upon incorporation of the peptide. As shown in Figure 6B, the S_{CD} profiles for the hCB$_1$(A118−L147) peptide and pure POPC were almost identical, and there was a characteristic profile of decreasing order toward the methyl group of the acyl chain in both the absence and presence of the peptide.

Spin−lattice relaxation times (T_{1Z}) provide information about molecular motions that occur on the time scale of the inverse Lamor frequency or even less. To probe the change

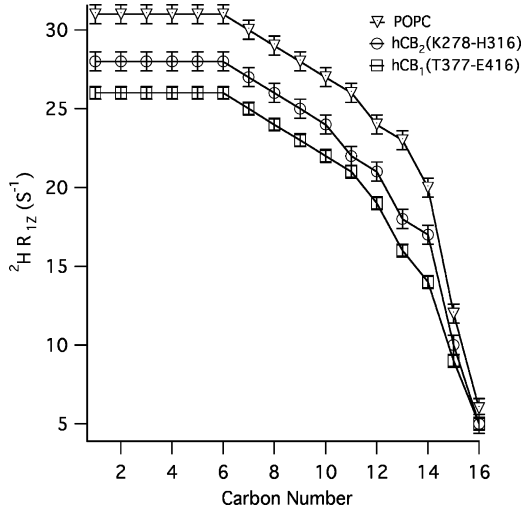

FIGURE 7: R_{1Z} relaxation measurements of POPC in the presence of cannabinoid peptides. ^{2}H relaxation rate measurements as a function of carbon position along the acyl chain for POPC with 1 mol % hCB$_1$(T377−E416) or with 1 mol % hCB$_2$(K278−H316) and POPC lipid bilayers prepared in the absence of peptide. R_{1Z} values were calculated from the peak intensities as a function of variable T delay at 30 °C. The uncertainty in the measurements is about $\pm$1 s^{-1} for triplicate data points.

in dynamic properties of the bilayer system upon peptide incorporation, the ^{2}H relaxation rates (R_{1Z}) were measured for the pure POPC bilayers using an inversion−recovery pulse sequence (Figure 7). Generally, R_{1Z} increased with carbon position along the acyl chain of POPC in all the systems studied. Pure POPC bilayers were more ordered when compared to those of the lipid/peptide mixture, as indicated by the longer R_{1Z} values of up to $\sim$31 $\pm$ 1 s^{-1}. Similarly, POPC with hCB$_1$(T377−E416) had the shortest R_{1Z} values ($R_{1Z} \sim 26 \pm 1$ s^{-1}), whereas the values of the POPC with hCB$_2$(K278−H316) ($R_{1Z} \sim 28 \pm 1$ s^{-1}) were intermediate between the POPC in the absence of the peptide and POPC with hCB$_1$(T377−E416). Therefore, the R_{1Z} measurements shown in Figure 7 compared consistently with the S_{CD} measurements presented in Figure 5. Thus, the overall R_{1Z} values of the lipid/peptide mixture support the order parameter profile.

Acyl chain methylene ^{2}H NMR spin−lattice relaxation rates have been observed to follow a square-law dependence on S_{CD} (*38*). In liquid crystal systems, R_{1Z} is directly proportional to S^2_{CD}, and such plots have been useful in distinguishing between the types of motion that modulate relaxation processes within the lipid bilayer (*39*). As shown in Figure 8, the relaxation rates are linearly related to S^2_{CD}. For pure POPC, the plot of R_{1Z} vs S^2_{CD} is linear but differs significantly from that of the POPC/peptide mixtures. The average intercept is about 1.5 $\pm$ 0.3 s^{-1} for all of the plots, and the slopes of the peptide-containing bilayers are significantly larger than that found for the pure POPC bilayers. The value of the slope for the pure POPC is 625 $\pm$ 18 s^{-1} and, in the presence of hCB$_2$(K278−H316) or hCB$_1$(T377−E416), is 752 $\pm$ 13 s^{-1} or 867 $\pm$ 11 s^{-1}, respectively.

DISCUSSION

The peptides corresponding to helix I, as well as helix VII and the juxtamembrane segment of the human cannabinoid receptors, hCB$_1$(A118−L147), hCB$_1$(T377−E416), and

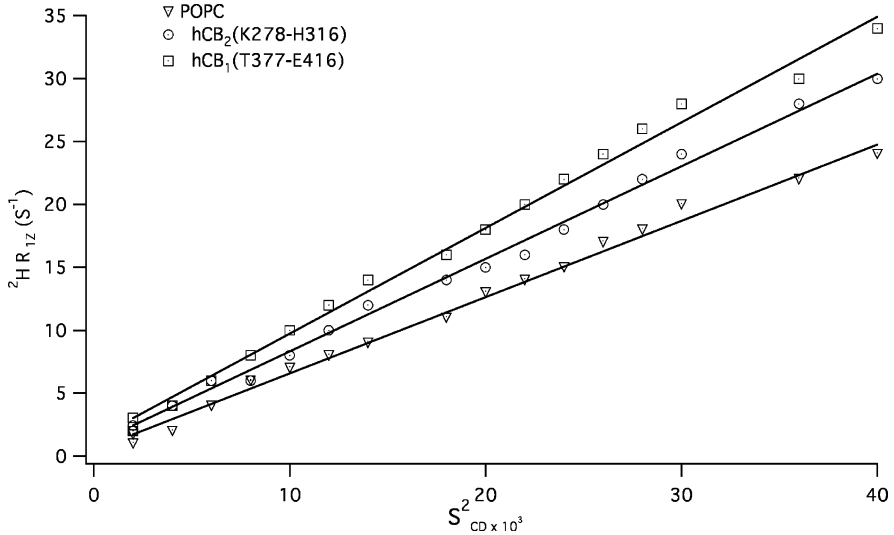

FIGURE 8: Plots of spin−lattice relaxation rates, R_{1Z}, vs S^2_{CD} for pure POPC and the POPC/peptide mixtures. The best linear fit plots are shown for POPC with 1 mol % hCB_1(T377−E416) or hCB_2(K278−H316) and POPC lipid bilayers prepared in the absence of peptide. The relaxation rates, R_{1Z}, as well as the order parameter, S_{CD}, were derived from the de-Paked spectra. The uncertainty in the data points is similar, with T_{1Z} error measurements of about ±11%.

hCB_2(K278−H316), were synthesized using solid-phase peptide synthesis. In the present study, the peptides were incorporated into phospholipid bilayers prepared from POPC. Solid-state NMR spectroscopy was used to monitor ^{31}P as a natural spin reporter on the headgroup of the POPC, as shown in Figures 2 and 3. The ^{31}P resonance signal coming from the lipid moiety has specific line shapes that can distinguish between the different phases formed from the model membrane, assuming that the phospholipid is the only source of endogenous ^{31}P (*35*, *38*, *40*). The POPC-d_{31} was labeled at the *sn*-2 acyl chain. The use of ^{2}H as a nonperturbing probe of the lipid moiety provided resonance assignment from the specific position of the deuterons along the lipid molecule, yielding detailed information about the segmental motional rates of the lipid and, consequently, about various interfacial phenomena. The following discussion explains (1) how the current solid-state NMR spectroscopic results support solution NMR data describing the structure of helix VIII, (2) the order of acyl chains, the amount of headgroup disruption, and membrane fluidity in terms of cannabinoid influence, and (3) a possible mechanism of cannabinoid action in biological systems.

Model of Helix VII and Helix VIII in the Lipid Membrane. Three concepts are used to describe the insertion of the transmembrane domain, helix VII, and the cytosolic segment, helix VIII, in the bilayer. The first and second concepts view helix VII to be transmembrane, whereas the cytosolic segment is viewed as either unstructured or structured but tethered to the membrane surface through palmitoylation at cysteine sites. A third concept describes a cytosolic helical segment that floats in the cytosol (*12*). In the current study, the bilayer can be described qualitatively from both the CSA of the ^{31}P NMR spectra (shown in Figures 2 and 3) and the perturbation of the acyl chains from the ^{2}H spectra (shown in Figure 4). The decrease in CSA of the ^{31}P spectra when either peptide was incorporated into the bilayer, as shown in Figures 2 and 3, suggests that CB_1 and CB_2 disrupt the bilayer in two ways. The first mode of headgroup disruption is due to an α-helical peptide lying on the membrane surface. The second mode of headgroup disruption is for the peptides to incorporate into the lipid environment, such that the transmembrane region comes into contact with the lipid hydrophobic core to minimize exposure to the aqueous surroundings. This causes a decrease in the ^{31}P CSA on the headgroup due to a fully spanning transmembrane peptide that disrupts the hydrophobic interaction in the headgroup region as the peptide enters and leaves the bilayer (*41*, *42*). The fact that the ^{2}H data display a perturbation of the acyl chains in a relatively constant way along the entire chain (each deuteron was distributed in a similar manner) supports the suggestion that a part of CB_1 and CB_2 peptides spanned the bilayer and interacted with the acyl chains. While these experiments do not provide the location of helix VIII of the peptides in the membrane, the ^{31}P and ^{2}H NMR data support transmembrane helix VII due to its disordering effect on the headgroup and the acyl chains. We hypothesize on the basis of the ^{31}P data and the solution NMR studies of helix VIII that helix VIII is structured and probably is not transmembrane (*43*). Thus, the extended peptide may have two distinct regions: a hydrophobic region which is inserted and spans the phospholipid bilayer and an amphipathic helix which is not transmembrane.

Bilayer Stability, Order, and Fluidity. One of the most remarkable observations made about this system was the stability of the bilayer at high peptide/lipid ratios. Static ^{31}P chemical shift anisotropy spectra at either a 1 or 4 mol % peptide concentration indicated that the bilayer was stable and intact, as shown in Figures 2 and 3. Accompanying the increase in the peptide/lipid ratio, there was an increase in the intensity of the small vesicles (diameter 500 ± 3 Å) as would normally be seen with other peptide systems (*33*). When comparing the percentage distribution of the vesicles between POPC with hCB_1(T377−E416) and POPC with hCB_2(K278−H316), it was evident that the former peptide destabilizes the bilayer more than the latter one. While the cause for the instability in the bilayer for this membrane system is not known, one factor could be due to the charged residues of helix VIII. To confirm this, we examined the difference in CSA between the two peptides when inserted in the bilayer (Figure 2C). Phospholipid headgroup perturba-

tion is often interpreted in terms of ^{31}P conformational changes within the phospholipid headgroup (*4*). There are two contiguous lysines close to the headgroup of the peptide, and both of these residues might cause conformational changes due to electrostatic interactions between the choline dipole and the net positive charge of the lysines (Figure 1). Roux et al. probed similar systems with a cationic integral membrane peptide flanked at both ends with two lysine residues (*44*). Their findings suggest that the residual membrane surface charge can induce a change in headgroup conformation, which can ultimately change the line shapes (*41*, *44*, *45*). At a neutral pH, the net charge on hCB_1(T377−E416) and hCB_2(K278−H316) is +2 and +3, respectively. The $-P-N^+$ dipole of the neutral phosphocholine headgroup, which is normally oriented almost 50° to the plane of the bilayer surface, can be altered in the presence of peptides or electrical charges, resulting in an increase in the ^{31}P CSA width (*42*, *45*). This interpretation is in good agreement with the observation that the ^{31}P CSA span of POPC with hCB_2-(K278−H316) (43 ± 1 ppm at 30 °C) with a net charge of +3 is larger than that of POPC with hCB_1(T377−E416) (41 ± 1 ppm at 30 °C) with a net charge of +2 (Figure 2C).

A second important observation came from the ^2H solid-state NMR spectra. The order parameters for each deuteron were determined on the basis of the quadrupolar splitting from the de-Paked ^2H spectra (Figure 5). In the pure POPC, the average order parameter was approximately 0.20 while in the presence of cannabinoid peptides, the system was less ordered [POPC with hCB_1(T377−E416), $S_{CD} \approx 0.16$, and POPC with hCB_2(K278−H316), $S_{CD} \approx 0.18$]. Several studies have been performed with both synthetic peptides and biologically expressed proteins in model membranes. These studies normally exhibited very small changes in acyl chain order and dynamics, especially at low peptide concentrations (*46*). Notably, even at a 1 mol % peptide/lipid ratio there was significant acyl chain disordering of the CB_1 and CB_2 peptides, possibly due to their mechanism of action.

One further observation of the acyl chain order was that the dramatic disordering effect of the acyl chain increased significantly in the central region of the phospholipid acyl chains, probably suggesting an increase in membrane fluidity (Figure 4A,B). However, as argued by Seelig and co-workers while membrane fluidity normally had little to do with the degree of ordering, it did affect the rate of motion of the acyl chains (*35*). To probe the rate of motion of the acyl chains (a measure of the fluidity of the membrane), ^2H R_{1Z} measurements were determined (Figure 7). The molecular motions were in the fast exchange limit for ^2H NMR (i.e., $>10^8$ s^{-1}). The molecular motions of the peptides incorporated into the phospholipid bilayers were consistent with the trends shown in the order parameter profiles. Thus, in the presence of the peptides, the R_{1Z} measurements confirmed that membrane fluidity was increased when either the CB_1 or CB_2 peptide was added to the membrane. Moreover, the membrane fluidity was increased more by the presence of the CB_1 than CB_2 peptide.

Additional insight into the dynamic behavior of the lipid acyl chain in the presence of the peptides was gained by comparing the plots in Figure 8. The motions of the lipid acyl chains can be distinguished as being fast or slow. The fast motions can cause either chain fluctuation (gauche−trans isomerization) or rotation about the long molecular axis, whereas the slow motions can contribute to bilayer deformation. At 1 mol %, the observation that R_{1Z} is proportional to S^2_{CD} was consistent with a lipid bilayer in the liquid-crystalline phase, dominated by fast motion involving chain fluctuations as well as acyl chain rotation along the long molecular axis. The pure POPC with the smaller slope suggested that the acyl chains pack more favorably than in the presence of the peptides. However, as the peptide concentration increased up to 6 mol %, the bilayer deformation complicated the dynamics of the acyl chains.

Biological Mechanism. We have demonstrated that the cannabinoid peptides perturbed the ^{31}P headgroups of the POPC bilayers (Figures 2 and 3), and on the basis of the POPC ^2H NMR spectra (Figure 4), the peptides also interacted with the side chain of the deuterated POPC bilayers. We have also demonstrated that the two peptides behave differently in the POPC phospholipid bilayers based upon the characteristics of their cytosolic regions. However, it is important to relate these characterization studies to those involving cannabinoid receptors in the biological system. First, Leterrier et al. showed that CB_1 undergoes constitutive endocytosis and recycling back to the plasma membrane in living cells (*47*). Endocytosis and recycling are important biological responses for most receptors such as those in the AT_1 angiotensin II receptor and the $5HT_{2C}$ serotonin receptor family (*48*, *49*). Previous studies have shown that the effects of protein interactions on lipids were achieved through a combination of electrostatic attractions as well as hydrophobic interactions between the peptide and lipid. These types of interactions tend to reduce local molecular motion. The finding that the peptides corresponding to CB_1 and CB_2 increased the degree of disordering within the bilayer suggested that these forces were not very strong. Though the current studies did not address the issue of endocytosis, we speculate that another possible mechanism of endocytosis and recycling is driven by the receptors' ability to increase membrane fluidity and permeability. Evidence for this includes the finding that both peptides decreased membrane fluidity differently, thus providing a manner in which CB_1 and CB_2 can perform their tasks in slightly different ways. Furthermore, through a mechanism not fully understood (possibly electrostatic stabilization of the cytosolic region on the membrane surface), both peptides corresponding to CB_1 and CB_2 destabilized the bilayer more than other structurally equivalent integral membrane proteins (*33*). The next question was how did synthetic peptides of other segments of the receptors behave in the POPC lipid bilayer environment? To this end, we tested the dynamics of POPC in the presence of hCB_1(A118−L147) (helix I) of CB_1 and found the results to be different from those seen in POPC with hCB_1(T377−E416) or POPC with hCB_2(K278−H316) (Figure 6). The S_{CD} profiles of POPC with hCB_1(A118−L147) were identical to the S_{CD} profiles of POPC. Thus, unlike the peptides corresponding to helix VII of CB_1 and CB_2, the S_{CD} profiles indicated that the former peptides indeed have significant influence on the properties of the POPC lipid environment. Whether this observation is unique to the cannabinoid receptors is uncertain and has yet to be tested with other GPCRs.

In conclusion, this study is the first to use solid-state NMR spectroscopy to investigate lipid/protein interactions of the peptides corresponding to the cannabinoid receptors (*50*).

The technique is well suited to sense the physical state of the lipid bilayer as well as the molecular motions associated with acyl chains in the presence of macromolecules. These studies indicate the possibility of determining helical orientation and dynamics in model membranes of the cannabinoid receptors by using solid-state NMR spectroscopy.

ACKNOWLEDGMENT

We gratefully acknowledge Dr. Jerome Groopman for overall support of this work and Dr. John Ladias for advice on this study. The NMR spectroscopy was carried out in the Department of Chemistry and Biochemistry, Miami University, Oxford, OH, and in the NMR Division, Bruker-Biospin Corp., Billerica, MA. We thank William Beavers at the Molecular Biology Core Facility, Dana-Farber Cancer Institute, for the synthesis and purification of the peptides. We also thank Janet Delahanty for editing the manuscript.

REFERENCES

1. Opella, S. J., and Stewart, P. L. (1989) Solid-state nuclear magnetic resonance structural studies of proteins, *Methods Enzymol. 179*, 242−275.
2. Opella, S. J. (1997) NMR and membrane proteins, *Nat. Struct. Biol. 4*, 845−848.
3. Kim, Y., Valentine, K., Opella, S. J., Schendel, S. L., and Cramer, W. A. (1998) Solid-state NMR studies of the membrane-bound closed state of the colicin E1 channel domain in lipid bilayers, *Protein Sci. 7*, 342−348.
4. Porcelli, F., Buck, B., Lee, D. K., Hallock, K. J., Ramamoorthy, A., and Veglia, G. (2004) Structure and orientation of pardaxin determined by NMR experiments in model membranes, *J. Biol. Chem. 270*, 45815−45823.
5. Waugh, J. S., Huber, L. M., and Haeberlen, U. (1968) Approach to high-resolution NMR in solids, *Phys. Rev. Lett. 20*, 180−182.
6. Pines, A., Gibby, M., and Waugh, J. S. (1973) Proton-enhanced NMR of spins in solids, *J. Chem. Phys. 59*, 569−590.
7. Barre, P., Zschoring, O., Arnold, K., and Huster, D. (2003) Structural and dynamic changes of the bindin B18 peptide upon binding to lipid membranes, *Biochemistry 42*, 8377−8386.
8. Cross, T. A. (1997) Solid state nuclear magnetic resonance characterization of gramicidin channel structure, *Methods Enzymol. 289*, 672−696.
9. Marassi, F. M., and Opella, S. J. (1998) NMR structural studies of membrane proteins, *Curr. Opin. Struct. Biol. 8*, 640−648.
10. Mascioni, A., Karim, C., Barany, G., Thomas, D. D., and Veglia, G. (2002) Structure and orientation of sarcolipin in lipid environments, *Biochemistry 41*, 475−482.
11. Watts, A., and Van Gorkom, L. C. M. (1992) The structure of biological membranes, in *Phospholipid Handbook* (Yeagle, P. L., Ed.) pp 307−336, CRC Press, Boca Raton, FL.
12. Howlett, A. C. (1998) The CB1 cannabinoid receptor in the brain, *Neurobiol. Dis. 5*, 405−416.
13. Kreitzer, A. C., and Regehr, W. G. (2001) Retrogade inhibition of presynaptic calcium influx by endogenous cannabinoids at excitatory synapses onto Purkinje cells, *Neuron 29*, 717−727.
14. Ohno-Shosaku, T., Maejima, T., and Kano, M. (2001) Endogenous cannabinoids mediate retrogade signals from depolarized postsynaptic neurons to presynaptic terminals, *Neuron 29*, 729−738.
15. Pertwee, R. G. (1997) Pharmacology of cannabinoid CB1 and CB2 receptors, *Pharmacol. Ther. 74*, 129−180.
16. Herkenham, M. (1992) Cannabinoid receptor localization in brain: relationship to motor and reward systems, *Ann. N.Y. Acad. Sci. 654*, 19−32.
17. Tsou, K., Brown, S., Sanudo-Pena, M. C., Mackie, K., and Walker, J. M. (1998) Immunohistochemical distribution of cannabinoid CB1 receptors in the rat central nervous system, *Neuroscience 83*, 393−411.
18. Pertwee, R. G. (1993) The evidence for the existence of cannabinoid receptors, *Gen. Pharmacol. 24*, 811−824.
19. Matsuda, L. A., and Bonner, T. I. (1995) Molecular biology of the cannabinoid receptor, in *Cannabinoid Receptor* (Pertwee, R. G., Ed.) pp 117−143, Academic Press, London.
20. Brown, A. D., and London, E. (2000) Structure and function of sphingolipid- and cholesterol-rich membrane rafts, *J. Biol. Chem. 275*, 17221−17224.
21. Sarker, K. P., and Maruyama, I. (2003) Anandamide induces cell death independent of cannabinoid receptors or vanilloid receptor 1: possible involvement of lipid rafts, *Cell Mol. Life Sci. 60*, 1200−1208.
22. Wakamatsu, K., Okada, A., Miyazawa, T., Ohya, M., and Higashijima, T. (1992) Membrane-bound conformation of mastoparan X, a G-protein activating peptide, *Biochemistry 31*, 5654−5660.
23. Xie, X.-Q., Chen, J.-Z., and Billings, E. M. (2003) 3D Model of the G-protein coupled CB2 cannabinoid receptor, *Proteins 53*, 307−319.
24. Bramblett, R. D., Panu, A. M., Ballesteros, J. A., and Reggio, P. H. (1995) Construction of a 3D model of the cannabinoid CB1 receptor: Determination of helix ends and helix orientation, *Life Sci. 56*, 1971−1982.
25. Palczewski, K., Kumasaka, T., Hori, T., Behnke, C. A., Motoshima, H., Fox, B. A., Le Tong, I., Teller, D. C., Okada, T., Stenkamp, R. E., Yamamoto, M., and Miyano, M. (2000) Crystal structure of rhodopsin: a G protein-coupled receptor, *Science 289*, 739−745.
26. Baldwin, J. M. (1993) The probable arrangement of the helices in G protein-coupled receptors, *EMBO J. 12*, 1693−1703.
27. Rigby, A. C., Barber, K. R., Shaw, G. S., and Grant, C. W. M. (1996) Transmembrane region of the epidermal growth factor receptor: behavior and interactions via ^{2}H NMR, *Biochemistry 35*, 12591−12601.
28. Davis, J. H., Jeffrey, K. R., Bloom, M., and Valic, M. I. (1976) Quadrupolar echo deuteron magnetic resonance spectroscopy in ordered hydrocarbon chains, *Chem. Phys. Lett. 42*, 390−394.
29. Massiot, D. F., Fayon, M., Capron, I., King, S., Le Calve, B., Alonso, J. O., Durand, B., Bujoli, Z. G., and Hoatson, G. (2002) Modelling one- and two-dimensional solid-state NMR spectra, *Magn. Reson. Chem. 40*, 70−76.
30. McCabe, M. A., and Wassall, S. R. (1995) Fast-Fourier-transform dePakeing, *J. Magn. Reson. B 106*, 80−82.
31. McCabe, M. A., and Wassall, S. R. (1997) Rapid deconvolution of NMR powder spectra by weighted fast Fourier transformation, *Solid-State Nucl. Magn. Reson. 10*, 53−61.
32. Davis, J. H. (1981) The description of membrane lipid conformation, order, and dynamics, *Biochim. Biophys. Acta 737*, 117−171.
33. Dave, P. C., Tiburu, E. K., Damodaran, K., and Lorigan, G. A. (2004) Investigating structural changes in the lipid bilayer upon insertion of the transmembrane domain of the membrane-bound protein phospholamban utilizing ^{31}P and ^{2}H solid-state NMR spectroscopy, *Biophys. J. 86*, 1564−1573.
34. Derome, A. E. (1987) Modern NMR techniques for chemistry research, in *NMR Spectroscopy: Data Acquisition* (Schorn, C., Ed.) 1st ed., pp 23−36, Pergamon Press, Oxford.
35. Seelig, J. (1978) ^{31}P nuclear magnetic resonance and the headgroup structure of phospholipids in membranes, *Biochim. Biophys. Acta 515*, 105−140.
36. Burnell, E. E., Cullis, P. R., and De Kruijtff, B. (1980) Effects of tumbling and lateral diffusion on phosphocholine model membrane ^{31}P-NMR lineshapes, *Biochim. Biophys. Acta 603*, 63−69.
37. Huber, T., Rajamoorthi, K., Kurze, V. F., Beyer, K., and Brown, M. F. (2002) Structure of decosahexaenoic acid-containing phospholipid bilayers as studied by ^{2}H NMR and molecular dynamics simulations, *J. Am. Chem. 124*, 298−309.
38. Paddy, M. R., Dahlquist, F. W., Dratz, E. A., and Deese, A. J. (1985) Simultaneous observation of order and dynamics at several defined positions in a single acyl chain using ^{2}H NMR of single acyl chain perdeuterated phosphatidylcholines, *Biochemistry 24*, 5988−5995.
39. Brown, M. F., Ribeiro, A. A., and Williams, G. D. (1983) New view of lipid bilayer dynamics from ^{2}H and ^{13}C NMR relaxation time measurements, *Proc. Natl. Acad. Sci. U.S.A. 80*, 4325−4329.
40. Cullis, P. R., and de Kruijff, B. (1979) Lipid polymorphism and functional roles of lipids in biological membranes, *Biochim. Biophys. Acta 559*, 328−339.
41. Wildman, K. A. H., Lee, D. K., and Ramamoorthy, A. (2003) Mechanism of lipid bilayer disruption by the human antimicrobial peptide, LL37, *Biochemistry 42*, 6545−6558.
42. Scherer, P. G., and Seelig, J. (1989) Electric charge effects on phospholipid headgroups. Phosphotidylcholine in mixtures with cationic and anionic amphiphiles, *Biochemistry 28*, 7720−7728.

43. Xie, X.-Q., and Chen, J.-Z. (2005) NMR structural comparison of the cytoplasmic juxtamembrane domains of G-protein-coupled CB1 and CB2 receptors in membrane mimetic dodecylphosphocholine micelles, *J. Biol. Chem. 280*, 3605−3612.
44. Roux, M., Neumann, J.-M., Hodges, R. S., Devaux, P. F., and Bloom, M. (1989) Conformational changes of phospholipid headgroups induced by a cationic integral membrane peptide as seen by deuterium magnetic resonance, *Biochemistry 28*, 2313−2321.
45. Hallock, K. J., Lee, D. K., and Ramamoorthy, A. (2003) MSI-78, an analogue of the magainin antimicrobial peptides, disrupts lipid bilayer structure via positive curvature strain, *Biophys. J. 84*, 3052−3060.
46. de Planque, M. R. R., Kruijtzer, J. A. W., Liskamp, R. M. J., and Marsh, D. (1999) Different membrane anchoring positions of tryptophan and lysine in synthetic transmembrane alpha helical peptides, *J. Biol. Chem. 274*, 20839−20846.
47. Leterrier, C., Bonnard, D., Carrel, D., Rossier, J., and Lenkei, Z. (2004) Constitutive endocytic cycle of the CB1 cannabinoid receptor, *J. Biol. Chem. 279*, 36013−36021.
48. Marion, S., Weiner, D. M., and Caron, M. (2004) RNA editing induces variation in desensitization and trafficking of 5-Hydroxytryptamine 2c receptor isoforms, *J. Biol. Chem. 279*, 2945−2954.
49. Miserey-Lenkei, S., Parnot, C., Bardin, S., Corvol, P., and Clauser, E. (2002) Constitutive internalization of active angiotensin II AT1A receptor mutants is blocked by inverse agonists, *J. Biol. Chem. 277*, 5891−5901.
50. Choi, G., Landin, J., and Xie, X.-Q. (2002) The cytoplasmic helix of cannabinoid receptor CB2, a conformational study by circular dichroism and ^{1}H NMR spectroscopy in aqueous and membrane-like environments, *J. Pept. Res. 60*, 160−177.

BI0525831